Atmospheric Environment 203 (2019) 1–9

Contents lists available at ScienceDirect

Atmospheric Environment

journal homepage: www.elsevier.com/locate/atmosenv

Characterization of $PM_{2.5}$-bound PAHs and carbonaceous aerosols during three-month severe haze episode in Shanghai, China: Chemical composition, source apportionment and long-range transportation

Xin-Yi Wei[a,b], Min Liu[a,b,*], Jing Yang[a], Wei-Ning Du[a], Xun Sun[a], Yan-Ping Huang[a], Xi Zhang[a], Saira Khan Khalil[a], Dong-Mei Luo[a], Ya-Dong Zhou[a]

[a] Key Laboratory of Geographic Information Science of the Ministry of Education, School of Geographic Sciences, East China Normal University, 500 Dongchuan Road, Minhang District, Shanghai, 200241, China
[b] Institute of Eco-Chongming (IEC), 3663 N. Zhongshan Rd., 200062, Shanghai, China

GRAPHICAL ABSTRACT

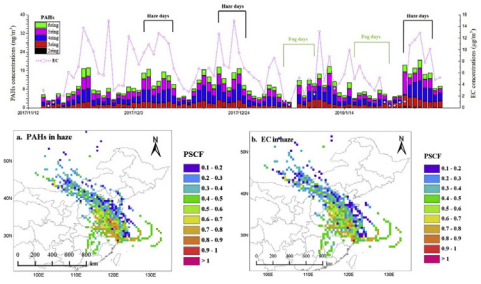

ARTICLE INFO

Keywords:
Polycyclic aromatic hydrocarbons
Carbonaceous aerosols
Haze episode
Source identification
Spatial transportation

ABSTRACT

To investigate the characterization of $PM_{2.5}$-bound polycyclic aromatic hydrocarbons (PAHs) and carbonaceous aerosols as well as the regulation of formation and transition in the haze episode, daily $PM_{2.5}$ samples (from Nov.2017 to Feb. 2018) were collected from an industrialized district in Shanghai, China. The average concentrations of PAHs and element carbon (EC) were 10.4 ± 4.55 ng/m^3 and 8.08 ± 2.97 μg/m^3 during haze episodes, which were 1.33 and 2.27 times higher than those during clear period, respectively. Secondary organic carbon (SOC) consisting of 52.2% organic carbon (OC) were the main chemical constitution of the aerosols resulting in heavy haze in Shanghai. Spearman correlation coefficient indicated that low temperature and relative humidity were the crucial factors attributing to the severe haze events. The Positive Matrix Factorization (PMF) model indicated that vehicle emissions (33.2%) were the predominant sources during haze period, followed by coal and biomass combustion (32.5%), coking (25.5%) and petroleum spill and leakages (8.87%). Zhejiang, Anhui and Jiangsu provinces were identified as potential major source areas of PAHs and EC according to potential source contribution function (PSCF) and concentration weighted trajectory (CWT) models. This study made contributions to target the prevention of pollutants in terms of severe haze event and long-range transportation as well as putting forward control measures and policies.

* Corresponding author. Key laboratory of Geographic Information Science of the Ministry of Education, School of Geographic Sciences, East China Normal University, 500 Dongchuan Road, Minhang District, Shanghai, 200241, China.
E-mail address: mliu@geo.ecnu.edu.cn (M. Liu).

https://doi.org/10.1016/j.atmosenv.2019.01.046
Received 5 October 2018; Received in revised form 16 January 2019; Accepted 19 January 2019
Available online 31 January 2019
1352-2310/

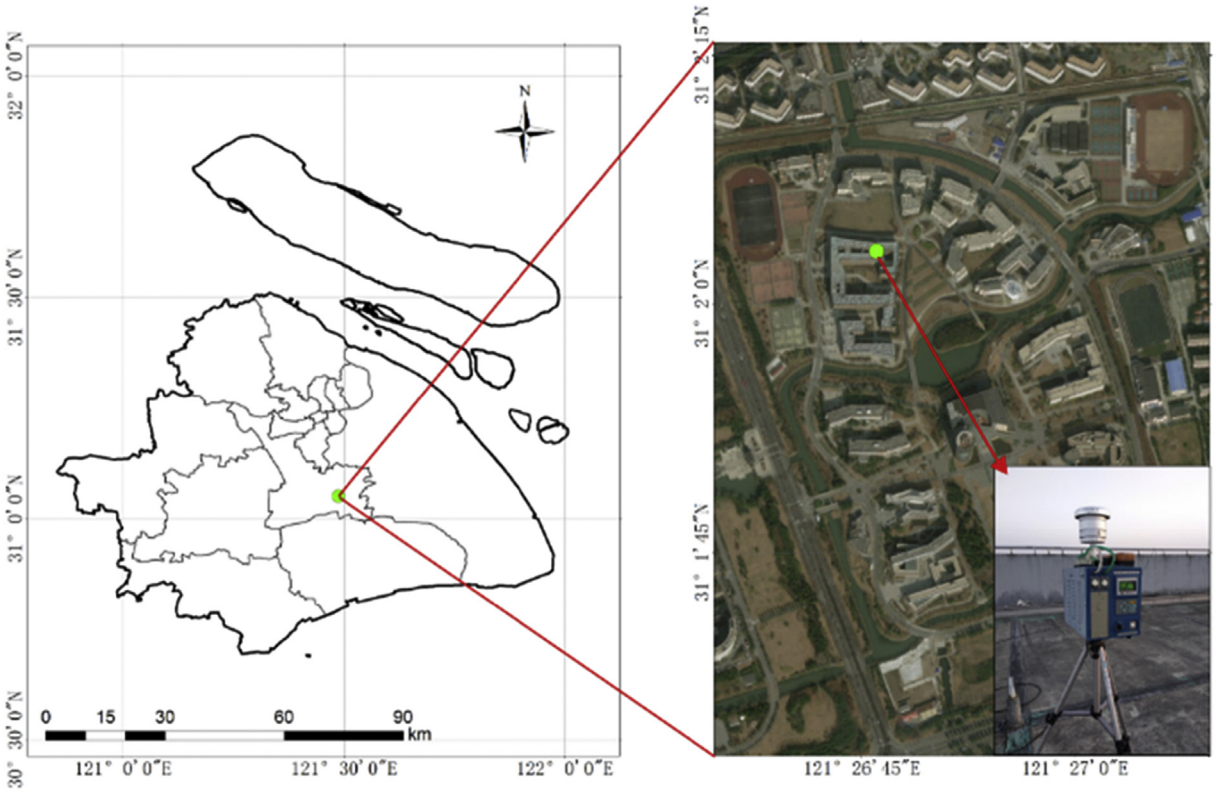

Fig. 1. The location of sampling station in Shanghai, China.

1. Introduction

Particulate matter (PM) has been extensively studied for its complicate source apportionment and adverse effects on human health. In-depth research on chemical composition of atmospheric PM is very crucial for classifying the particle toxicity and its role in environmental pollution (Yang et al., 2011). The essential components of PM such as polycyclic aromatic hydrocarbons (PAHs), carbonaceous aerosols including organic carbon (OC) and element carbon (EC), have drawn great concern in today's generation due to their homology, carcinogenicity and severe health problems such as cardiovascular, cardiopulmonary and respiratory disease (Smith et al., 2009).

EC, also referred as black carbon (BC), is released from the incomplete coal combustion, biomass burning, natural gas and fossil fuels (Hildemann et al., 1991). OC is mainly derived from primary and secondary process. Primary OC is directly emitted from combustion source, while secondary organic carbon (SOC) is due to chemical transformation process. Once emitted into the air, the carbonaceous aerosols can be transported in the regional or global scale. So the research on long-range transportation and the knowledge of SOC estimation are important for understanding the impacts of regional emissions.

PAHs are abundantly generated from uncompleted combustion of fossil fuels and biomass as well as unburnt petroleum (Vander Wal et al., 2007). PAHs adsorbed in $PM_{2.5}$ can be transported in the atmosphere to remote regions and they are ubiquitous in the environment. Thus, the research on source apportionment of $PM_{2.5}$-bound PAHs is significant to elucidate its potential emission and pollution process. The methods such as chemical mass balance (CMB) (Li et al., 2003), principal component analysis (PCA) (Simcik et al., 1999; Li et al., 2016), positive matrix factorization (PMF) (Sofowote et al., 2008) have been widely applied to qualitatively or quantitatively identify the source apportionment of PAHs in $PM_{2.5}$. In addition, considering its cross-regional migration accompanied with air mass, numerous studies have also used the potential source contribution function (PSCF) as well as concentration and weighted trajectory (CWT) models to investigate the long-range transportation of $PM_{2.5}$-bound PAHs during the severe haze episode (Dimitriou and Kassomenos, 2015).

With rapid industrialization, urbanization and economic development during past few decades, haze, an atmospheric phenomenon in which dust, smoke, and other dry particulates obscure the clarity of the sky, has resulted in a serious impact on East China especially during winter severe haze episode (Huang et al., 2014). In particular, the Yangtze River Delta (YRD) has a frequent incidence of haze, which was dominantly influenced by heavy concentration of $PM_{2.5}$. The PM-dominated haze problem in Shanghai - the economic and financial center of YRD has become increasingly severe and frequent, arousing growing attention for the past few decades (Zhang et al., 2015). Recently, several researchers have successfully explored the composition characteristics and source apportionment of pollutants in PM during four seasons (Wang et al., 2016; Liu et al., 2018).

Nevertheless, until now, there is still a limited understanding on some essential issues during the procedure of severe haze episode formation, such as the accumulation and transition of target contaminations (PAHs, OC and EC), the driving factors for soaring secondary aerosols, and the mechanism on EC-PAHs interaction. Although the environmental behavior and eco-toxicology of PAHs were largely influenced by carbonaceous aerosols (Gustafsson et al., 1997), among most studies on $PM_{2.5}$-bound pollutants, few took it into consideration. Therefore, to attain a better comprehension of the formation and transition mechanism of severe haze episode, a detailed investigation was implemented on particle-associated carbonaceous aerosols and PAHs during the typical haze episodes in Shanghai. The major objectives of this study were (1) to reveal the temporal variations of concentrations of $PM_{2.5}$-bound PAHs and carbonaceous aerosols during the haze, fog and clear period; (2) to explore the relationship between OC, EC and estimate the secondary organic carbon (SOC) based on the method of EC-tracer; (3) to investigate the regulation of EC-PAHs interaction during severe haze episode and the relationship between

PAHs, carbonaceous aerosols concentrations and meteorological parameters; (4) to identify pollution sources by PMF model and HYSPLIT model in terms of tracking the long-range transportation of potential source regions.

2. Materials and methods

2.1. Study area and sample collection

As is illustrated in Fig. 1, the sampling site is selected in Minhang campus of East China Normal University (ECNU), which is situated in the suburban area of Shanghai. The low-densely residential districts are distributed at its north and southwest directions within about 1 km. The sampling site faces two main highways with heavy traffic (1.2 km in the northeast and 1.8 km in the west, respectively). A thermal power plant was located 3 km away from studying site. The sampling station was installed on the roof of the five-story building (about 20 m above the ground level).

The sampling period maintained from November 2017 to February 2018 which included 21 haze days, 20 fog days and 50 clear days. $PM_{2.5}$ samples were collected by an automatic $PM_{2.5}$ sampler (2050 intelligent $PM_{2.5}$, Qingdao Laoying Environmental Technology Institute) with a flow rate of 100 L/min from 12:00 at noon each day and lasted for about 24 h. A total of 91 samples were consecutively collected during the three-month severe haze period on quartz fiber filters (Whatman Company, with diameter of 90 mm). All filters were baked at 450 °C for 4 h and kept in aluminum foil envelopes before sampling. The filters were weighted before and after sampling by a microbalance (balance sensitivity: ± 0.010 mg) under the condition of constant temperature (20 °C) and relative humidity (50%). Then all filters were stored in the freezer at −20 °C until chemical analysis.

2.2. Chemical analysis

A quarter of the $PM_{2.5}$ sampling filter was added together with 2 g diatomite (disperse samples) and 0.5 g copper powders (remove elemental sulfur), which were extracted with dichloromethane and acetone (1:1, v/v) by using an accelerated solvent extractor (ASE350, Thermo Fisher, US).

The 200 ng surrogate standard (terphenyl-d_{14}) was added as a recovery indicator after extraction and the further purification was carried on by rotary evaporator (S-EVAP-RB, Orgragation, USA) and column with amorphous sodium sulfate, silica gel and alumina. The elute solvent was 15 mL hexane and 70 mL hexane-dichloromethane (3:7, v/v). A 200 ng mixture of naphthalene-d_8, acenaphthene-d_{10}, phenanthrene-d_{10}, chrysene-d_{12}, and perylene-d_{12} as internal standards were added to the final samples. The ultimate extracts were concentrated to 1 mL and stored into a 2 mL GC bottle (sealed with parafilm) at −20 °C in refrigerator for the subsequent quantitative analysis.

The concentrations of 16 PAHs prioritized by the US Environmental Protection Agency (EPA) were detected by using a gas chromatograph-mass spectrometer (Agilent 7890B GC-5977A MS), which was set up in the selective ion monitoring (SIM) mode: naphthalene (Nap), acenaphthene (Ace), acenaphthylene (Acy), fluorene (Fl), phenanthrene (Phe), anthracene (Ant), fluoranthene (Flu), pyrene (Pyr), Benz[*a*]anthracene (BaA), chrysene (Chr), benzo[*b*]fluoranthene (BbF), benzo[*k*]fluoranthene (BkF), benzo[*a*]pyrene (BaP), indeno[1,2,3-*cd*]pyrene (InP), Dibenz[*a,h*]anthracene (DahA), and benzo[*ghi*]perylene (BghiP). The temperature of oven was set at 55 °C holding for 2 min, then heated to 280 °C at a rate of 20 °C/min and held for 4 min, and finally increased to 300 °C at a rate of 3 °C/min holding for 4 min.

The concentrations of OC and EC were determined by a thermal and optical carbon analyzer (the DRI Model 2015) following Interagency Monitoring of Protected Visual Environments (IMPROVE-A) thermal/optical reflectance protocol. Four OC fractions consisting of OC1 (140 °C), OC2 (280 °C), OC3 (480 °C) and OC4 (580 °C), three EC fractions consisting of EC1 (580 °C), EC2 (740 °C), and EC3 (840 °C) were supplied and the part converting pyrolytically from OC to EC (OPC) was considered. The IMPROVE protocol defines the sum of OC as OC1 + OC2 + OC3 + OC4 + OPC, EC as EC1 + EC2 + EC3-OPC, TC as OC + EC (Chow et al., 2004).

2.3. Quality assurance and quality control

The quality assurance and quality control (QA/QC) were conducted as follows: (1) Surrogate standard recovery analysis. After the GC-MS quantitative analysis, the concentrations of PAHs and surrogate standards were measured depending on the added internal standard concentration (200 μg/L) as well as the relative response factors of target compounds. The average recoveries of surrogate standard ranged from 83.5% to 108.7%. (2) Replicate analysis. The PAHs concentrations' variation coefficient was < 8% while comparing two duplicate samples which were conducted in the same way for each batch of 10 samples. (3) Standard-addition in blank and matrix. The average recoveries of PAHs standards along with method blank and matrix were 67.3–104% and 71.1–97.5%, respectively. The concentrations of the detected 16 PAHs were rectified by deducting the method blank value and corrected according to the recovery efficiency based on surrogate standard.

In terms of the carbonaceous aerosols, ten blank filters were determined and the results were rectified by the average value of blank sample. The detection limit was below 1.0 μg/m^3 for EC and OC. Replicate analysis were performed one in every 5 samples and the errors are below 8%, 8%, 10% for TC, OC and EC, respectively.

2.4. Meteorological factors

During the sampling period, meteorological parameters including temperature (T, °C), wind speed (WS, m/s), relative humidity (RH, %) and visibility (VS, km) were correspondingly recorded from Weather Underground (https://www.wunderground.com/). According to China Meteorological Administration (CMA), haze is defined as VS < 10 km and RH < 80% while fog is defined as VS < 10 km and RH > 90%. For VS > 10 km, it is clear day. Haze, fog and clear days accounted for 23% (21 days), 22% (20 days) and 55% (50 days) during the whole observation periods, respectively. Table S1 illustrated the time series of the meteorological parameters and present the variation between haze, fog and clear period. The lowest average wind speed (10.48 m/s) and relative humidity (73.52%) were occurred during haze period which provided the favorable condition for the accumulation of pollutants. While the lower average temperature (6.5 °C), higher relative humidity (95.20%) and wind speed (15.15 m/s) during fog period were more inclined to the transportation and diffusion of contaminants.

2.5. Methodology analysis

2.5.1. PMF model

PMF model is a superior receptor model which can be applied for the identification of sources and quantifications of their contributions to the target compounds (Sofowote et al., 2008). The PMF model was described by equation as follows:

$$x_{ij} = \sum_{k=1}^{p} g_{ik} f_{kj} + e_{ij} \quad (1)$$

$$Q = \sum_{i=1}^{n} \sum_{j=1}^{m} \left(\frac{x_{ij} - \sum_{k=1}^{p} g_{ik} f_{kj}}{u_{ij}} \right)^2 \quad (2)$$

where x_{ij} represents the concentrations of compound j in sample i, p is the factor number, g_{ik} represents a mass of factor k contributing to compound i, f_{kj} stands for the fraction of compound j in factor k, e_{ij} is the residual of compound j in sample i, u_{ij} represents the uncertainty

Table 1
The concentrations of target pollutants in $PM_{2.5}$ during study period (haze, fog, clear period) in Shanghai.

Species		$PM_{2.5}$ (μg/m^3)	PAHs (ng/m^3)	LMW PAHs (ng/m^3)	HMW PAHs (ng/m^3)	EC (μg/m^3)	OC (μg/m^3)	TC (μg/m^3)	OC/EC
Total	Mean ± SD	53.6 ± 35.9	12.3 ± 10.9	3.8 ± 6.9	8.5 ± 5.5	6.3 ± 3.9	12.0 ± 5.8	18.3 ± 9.3	2.4 ± 1.4
	Range	10.0–189.0	2.2–68.7	0.5–42.1	1.6–27.1	0.3–15.0	1.9–29.9	2.2–41.7	0.9–11.5
Haze	Mean ± SD	92.9 ± 44.4	10.4 ± 4.6	1.9 ± 0.9	8.5 ± 3.9	8.08 ± 3.0	14.7 ± 5.5	22.8 ± 7.9	1.9 ± 0.5
	Range	30.0–189.0	3.8–20.5	0.5–2.8	3.7–16.8	3.03–12.9	4.6–25.9	7.6–38.7	0.9–3.2
Fog	Mean ± SD	34.5 ± 24.6	7.8 ± 4.8	2.0 ± 1.4	5.8 ± 3.6	3.57 ± 3.4	8.3 ± 6.6	11.9 ± 9.8	3.4 ± 2.3
	Range	10.0–94.0	2.2–18.4	0.6–5.5	1.6–12.9	0.4–11.7	2.2–29.9	2.7–41.7	1.3–11.5
Clear	Mean ± SD	44.8–21.0	14.9 ± 13.6	5.4 ± 9.0	9.5 ± 6.4	6.67 ± 3.8	12.3 ± 4.9	19.0 ± 8.4	2.2 ± 0.8
	Range	17.0–126.0	3.1–18.7	0.7–42.1	1.7–27.1	0.33–15.0	1.88–23.9	2.2–38.9	1.1–5.7

associated with x_{ij}, n is the number of samples, and m is the number of compounds.

The uncertainty of the PAH concentrations was measured on the basis of the method detection limit (MDL) and measurement error fraction. MDL was defined as triple standard deviation of PAH concentrations in 10 method blank samples, in the range 0.002–0.026 ng/m^3 for all monitored PAHs. If the concentrations of PAHs are less than the corresponding MDL, the uncertainty value is calculated as 5/6 of MDL. While the concentration is greater than the MDL, the uncertainty value is calculated as formula 4:

$$u = \begin{cases} \frac{5}{6} \times MDL, & x_{ij} \le MDL_j, \quad (3) \\ \sqrt{(error\ \ fraction \times concentration)^2 + (MDL_j)^2}, & x_{ij} > MDL_j. \quad (4) \end{cases}$$

Naphthalene was categorized as "bad" (signal/noise (S/N) ratio < 2) which was excluded from the model for the sake of its volatilization. An extra modeling uncertainty of 5% was set. The S/N ratios of all other compounds were greater than two, which were categorized as "strong" due to their satisfactory fitting results. In addition, the contribution of each source to total PAH concentrations was obtained by the multiple linear regression analysis with forward stepwise method.

2.5.2. Back-trajectory calculation

The backward trajectories were calculated by applying HYSPLIT model (NOAA Air Resource Laboratory) (Kong et al., 2014). The model was run every 6 h at the beginning of 00:00, 06:00, 12:00 and 18:00 UTC each day, which was driven by the Global Data Assimilation System (GDAS) meteorological dataset (1° × 1°). The duration of calculating air mass backward trajectories was 72 h while the starting height was 500 m above ground level. The results of HYPSPLIT model were preserved as endpoint files. For further trajectory analysis and clustering, the results were imported into software Meteolnfo (http://www.meteothinker.com).

2.5.3. PSCF and CWT algorithms

Potential source contribution function (PSCF, TrajStat) model was analyzed to identify the spatial source areas of PAHs and EC, which connected the transport pathway of backward trajectory with concentrations of contaminants (Nicolás et al., 2011). The study region was divided into equal $i \times j$ grid cells (ij) and the value of PSCF is defined as:

$$PSCF_{ij} = \frac{m_{ij}}{n_{ij}} \quad (5)$$

where i and j represent the latitude and longitude, while the number of endpoints through the ij cell was defined as n_{ij}. The number of endpoints concentrated on the same cell that exceeded the criterion value (the 75th percentile for each target compound) was designated as m_{ij}. In order to reduce the uncertainty in cells by decreasing the effect of small n_{ij} value, the value of PSCF was multiplied with an arbitrary weighting function W(n_{ij}) as follows (Wang et al., 2009):

$$W(n_{ij}) = \begin{cases} 1.00, & 3n_{mean} < n_{ij} \\ 0.70, & 1.5n_{mean} < n_{ij} \le 3n_{mean} \\ 0.40, & n_{mean} < n_{ij} \le 1.5n_{mean} \\ 0.20, & n_{ij} < n_{mean} \end{cases} \quad (6)$$

The concentration-weighted trajectory (CWT) model was also applied to weight trajectories with target compounds, which had the advantage of distinguishing the moderate pollutant source from the strong one. The studied domain was in the range of 15° N to 65° N and 85° E to 145° E with the resolution of 1.0° × 1.0°, which contains almost all regions overlaid with entire airflow transport pathways. The CWT can be defined as:

$$C_{ij} = \frac{\sum_{h=1}^{M} C_h \times \tau_{ijh}}{\sum_{h=1}^{M} \tau_{ijh}} \times W(n_{ij}) \quad (7)$$

where C_{ij} is the average weighted concentration of the back-trajectory h in the ij cell. M is the whole number of trajectories. C_h represents the arrival of trajectory h's pollutants contents. τ_{ijh} is the time spent in the ij cell that trajectory h remains. Both PSCF and CWT algorithms were calculated by applying the MeteoInfo software-TrajStat Plugin (Wang et al., 2009), which had been certified effective to designate the potential source regions of pollutants.

3. Results and discussions

3.1. Temporal variation of OC, EC concentrations and SOC formation

As illustrated in Table 1, daily OC concentrations ranged from 4.60 to 25.9 μg/m^3 and from 1.88 to 23.9 μg/m^3 during haze and clear period, respectively. EC concentrations varied from 3.03 to 12.9 μg/m^3 during haze period and from 0.33 to 15.0 μg/m^3 during clear period, respectively. The average concentrations of EC exhibited the trend as haze (8.08 μg/m^3) > clear (6.67 μg/m^3) > fog (3.57 μg/m^3), and the one-way Analysis of Variance (ANOVA) indicated the significant variation ($p < 0.01$) of contamination degree between haze period and fog period. This was in accordance with the result found by (Zhou et al., 2013) that the concentrations of EC during the haze period were significantly higher than other study period.

As illustrated in Table S2, the concentrations of EC were comparable to Beijing (7.5 μg/m^3, China) and the values were slightly lower than that measured in Nanjing (10.4 μg/m^3, China) (Chen et al., 2010) and Mumbai (7.3 μg/m^3, India) (Joseph et al., 2012). However, the concentrations were significantly higher than those in developed countries. For example, as was reported in Barrado et al. (2012) and Park et al. (2012), the mean values of EC were 0.106 μg/m^3 and 1.8 μg/m^3 in Spain and Seoul, respectively.

The ratio of particulate OC to EC was an essential index that indicated the source type and intensity (Blando and Turpin, 2000). It showed the correlations between OC and EC by separating the OC/EC ratios into three groups (> 2.5, 1.5–2.5, and < 1.5) for all $PM_{2.5}$ samples during the study period (Fig. S1a). Almost 65% of the OC/EC ratios showed the relatively low ratios (1.5–2.5), indicating the contribution

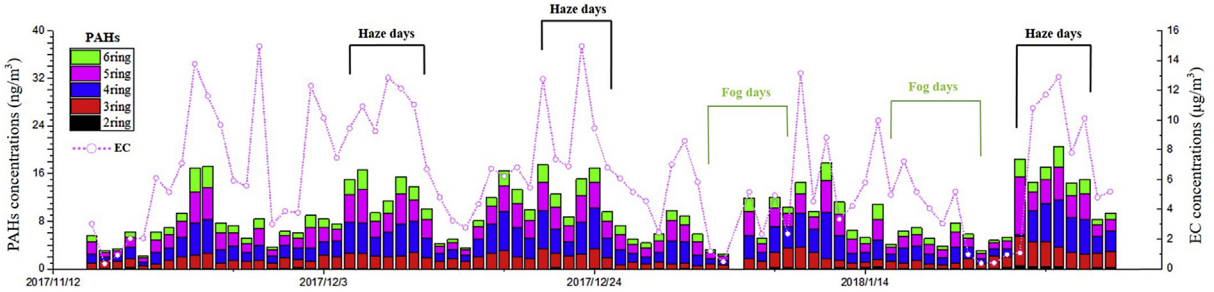

Fig. 2. Time series of $PM_{2.5}$-bound PAHs (with different rings) and EC mass concentrations during haze, fog period and clear period.

of vehicular emissions on the severe haze in the area (Chow et al., 2005). In addition to the intensive traffic emission, the higher ratio (> 2.5) of OC/EC was related to the rapid transformation of the SOC precursors such as volatile organic compounds (VOCs) due to the existing of the thermal power plant nearby the sampling station. So that precursors were more inclined to be transformed to SOC, causing the higher OC/EC.

Scatter plots of OC and EC and their correlation coefficients during different periods are illustrated in Fig. S1b. The correlation coefficients of OC and EC during study period showed the trend of fog ($r = 0.85$) > clear ($r = 0.72$) > haze ($r = 0.51$), indicating the growing SOC generation along with the increase of pollution degree. During the non-haze period, strong correlations between OC and EC suggested that they may derive from the similar sources. However, in the severe haze episode, the dispersion through long-range transport, the stagnant meteorological condition, and aging effect under sunlight irradiation may all result in the decrease of EC concentrations and the secondary formation of OC. So the correlation coefficients of OC and EC reduced correspondingly.

The contributions of primary and secondary organic carbon to carbonaceous aerosol can be evaluated from the following equations (Turpin and Huntzicker, 1995):

$$OC_{pri} = EC \times (OC/EC)_{min} \quad (8)$$

$$OC_{sec} = OC_{total} - (OC/EC)_{minimum} \times EC \quad (9)$$

where OC_{pri} is primary OC, $(OC/EC)_{min}$ is the minimum ratio of OC/EC, OC_{sec} is secondary OC, OC_{total} is total OC.

As presented in Table S3, the SOC concentrations were 8.08 ± 3.81, 3.90 ± 3.00 and 5.40 ± 2.51 μg/m^3 during the haze, fog, and clear period while the fraction of SOC accounted for 52.2%, 40.8% and 32.1% of OC, respectively. The highest percentage (52.2%) of SOC during haze period could result from photochemical activity and low atmospheric temperature. These results were well in accordance to the conclusions acquired by Chen et al. (2017).

3.2. Temporal variation of PAH concentrations

The average concentration of 16 priority $PM_{2.5}$-bound PAHs (Σ_{16}PAHs) during haze period was 10.4 ng/m^3, which was about 1.33 times higher than that during fog period (7.80 ng/m^3). In detail, PAH concentrations ranged from 3.80 to 20.5 ng/m^3, 2.18–12.4 ng/m^3 and 3.12–18.7 ng/m^3 during haze, fog, and clear periods, respectively. There was no significant difference between the haze with clear period ($p > 0.05$). This could be attributed to the various factors (e.g., pollutant emission, meteorological parameters and chemical degradation) resulting in the fluctuation of particulate PAH concentrations (Schauer et al., 2003). To be concrete, it can be mainly attributed into three parts: 1. The pollutant emission, especially industrial coal combustion, vehicle emissions and biomass burning for heating through long-range transportation. 2. The stagnant meteorological condition and low-relative humidity are prone to the accumulation and maintenance of $PM_{2.5}$-bound pollutants. 3. The elimination process caused by photochemical reaction and wet deposition may reduce the concentration especially during the fog period. The average concentrations of 7 carcinogenic PAHs (BaA, Chr, BkF, BbF, BaP, DahA and InP, Σ_7PAHs) were 5.94, 4.12, and 6.29 ng/m^3 during haze, fog, and clear period, accounting for 43.0–67.4%, 37.5–64.4% and 13.8–67.9% of Σ_{16}PAHs with the mean of 57.0%, 52.5% and 50.1%, respectively. The increasing proportion of carcinogenic PAHs from clear to haze period can attribute to their low solubility and volatility, implying that the more severe pollution may result in the relatively more profound carcinogenic influence on human health when compared with that in the fog period. As illustrated in Table S4, in comparison to $PM_{2.5}$-bound PAHs pollution in this study with domestic and overseas cities, it presented the moderate pollution level. More concretely, the concentration of PAHs in Shanghai was much higher than that in Spain (0.106, 1.05 ng/m^3), USA (0.98 ng/m^3) and Italy (0.14 ng/m^3). However, the contents were remarkably lower than other developing country such as Turkey (88.4 ng/m^3).

As depicted in Fig. 2, the variations of relative percentage with different rings of PAHs during whole period indicated the trend of 4 ring (31.1%) > 3 ring (29.7%) > 5 ring (24.0%) > 6 ring (13.7%) > 2 ring (1.5%). During haze period, the dominant PAHs were 4 ring with the average concentrations of 3.73 ng/m^3, accounting for 36.0% of Σ_{16}PAHs. Whereas 2 ring PAHs contributed least to total PAHs (0.09 ng/m^3, 0.82%). In addition, the dominant PAHs were 5 ring and 3 ring during fog and clear period, respectively, probably mainly attributed to the variation of meteorological conditions and corresponding chemical reaction during different period. For example, the stagnant environment increased the formation of secondary aerosols, which offered the favorable media to absorbed the corresponding PAHs. The relatively high temperature may more likely to induce the photochemical reaction, which may result in the degradation of high molecular PAHs. And the influences of industrial and anthropogenic activities were also expected to vary (i.e. vehicle emission, coal burning, petroleum leakage).

3.3. Correlation analysis between target pollutants and meteorological parameters

Significant correlations between Σ_{16}PAHs and carbonaceous aerosols (OC, EC, OC/EC) were observed during haze ($r > 0.83, p < 0.01$) and fog ($r > 0.58, p < 0.01$) period (Table S5). These indicated that the correlations were significantly enhanced with the increase of pollution level as well as the sorption and desorption of PAHs on carbonaceous aerosols. However, there was no significant relationship during clear period.

High molecular weight (HMW) PAHs showed especially significant correlations with carbonaceous aerosols (EC, OC, TC), particularly during the haze period ($p < 0.01$, $r = 0.847$, 0.836, 0.900, respectively).

The results during fog period were similar to those during clear period. However, 5-ring PAHs didn't show the significant correlations with carbonaceous aerosols while 3-ring PAHs got relatively higher

values in correlation with EC and OC. In comparison, there were no significant correlations between carbonaceous aerosols and low molecular weight (LMW) PAHs during the whole period, especially naphthalene (2-ring PAHs), which may result from its instability and volatility (Tan et al., 2011). Excluding the clear period, the correlations of $PM_{2.5}$-bound LMW PAHs with both OC and EC were significantly enhanced ($p < 0.01$ for haze period; $p < 0.05$ for fog period), indicating that LMW PAHs were also carried by carbonaceous aerosols during severe haze to some extent. On the other side, 4-ring PAHs showed significant correlations with all carbonaceous pollutants. Hence, although not all PAHs were associated with carbonaceous aerosols, they also played an important role in carrying PAHs, especially the HMW PAHs during the severe haze period. This conclusion was in accordance with a previous study in which considerable PAHs were adsorbed in carbonaceous pollutants (Wang et al., 2014).

The correlation analysis between the meteorological parameters and the atmospheric pollutants (PAHs, EC and OC) was illustrated in Table S6. The spearman correlation coefficients of PAH concentrations and temperatures during haze and clear period were -0.664 ($p < 0.01$) and -0.562 ($p < 0.01$), respectively, while the coefficients were -0.500 ($p < 0.05$) during haze period between TC concentrations and temperatures. The result was in accordance with the conclusion that the lower temperature was prone to resulting in the haze weather (Tsang et al., 1988). However, the haze episode on one hand can be easily formed by the low temperature. On the other hand, as the severe haze may reduce the solar radiation, the temperature will decrease correspondingly. So there was a reciprocal causation relationship between the severe haze episode and atmospheric temperature. Relative humidity showed the negative correlation with PAHs ($r = -0.561$, $p < 0.01$) and TC ($r = -0.375$, $p < 0.05$) concentration during the fog period ($r = 0.397$, $p < 0.05$). During haze period, the negative relationship may because by: (1) the stagnant meteorological condition; (2) the removal of atmospheric particulates by wet deposition; (3) the accumulation of $PM_{2.5}$-bound pollutants during dry period. However, during the fog period, higher relative humidity may be more inclined to the formation of pollutant concentration and the impact may be even greater than that from the aerosol particles especially in the heavy fog weather. The correlation coefficients between target pollutant concentrations and other pollutants (SO_2, NO_2, CO, O_3) were calculated by different period. It showed the better relationship between PAHs ($r = 0.523$, $p < 0.01$), TC ($r = 0.386$, $p < 0.05$) and SO_2 during haze period than the clear period ($r = 0.210$, $p < 0.05$, $r = 0.364$, $p < 0.01$). In terms of NO_2 and CO, there were positive correlation with carbonaceous aerosols while there was no significant correlation with PAHs. It indicated that EC, NO_2 and CO mainly derived from the similar sources such as diesel and gasoline vehicles emission (Pio et al., 2011). The negative correlation between carbonaceous aerosols and O_3 was found during the clear period. However, there was no significant correlation during haze period, which may result from the increased atmospheric oxidation and the formation of SOC.

3.4. Source apportionment

In this study, PMF model was used to illustrate the source apportionment of $PM_{2.5}$-bound PAHs. The statistics were input into PMF model during haze, fog and clear period, respectively, which consisted of 21, 20 and 50 sets of data and 16 PAH compounds. The base model was run 20 times and four factors were obtained. In addition, the contributions of contaminants on each factor, the quantitative ratio of emission sources, and their temporal variations were analyzed and compared during different periods.

During the haze period, the first factor had the high loading of Acy, Ace and Fl, which were the indicators for leakage and volatilization of crude oil and petroleum products (Marr et al., 1999) (Fig. S2). In addition, the volatilization from oil-contaminated river (within 3 km from sample sites) may also result in the increasing pollution of low molecular weight PAHs such as Acy and Ace. So the first factor can be interpreted as the petroleum spill and leakages. The second factor was mainly composed of BbF, BkF, BaP, DahA and InP. High molecular weight PAHs such as DahA and InP were the major PAHs in vehicle exhausts (Motelay-Massei et al., 2007). BbF and BkF can be regarded as the tracer of diesel-powered vehicles (Marr et al., 1999), and BaP was mainly identified as the powered traffic emission (Li and Kamens, 1993). Therefore, the second factor can be concluded as the source of vehicle emissions. The third factor predominantly consisted of Nap, Flu and Pyr which were often used as markers of emissions from coal combustion and biomass emission (Kulkarni and Venkataraman, 2000). Hence, this factor can be attributed to the source of coal and biomass combustion. The fourth factor was found to be rich in Phe, Ant, BaA and Chr. Phe and Ant was identified as the impact of coking while BaA and Chr was mostly regarded as the indicators of coke oven emissions (Aydin et al., 2014). So the fourth factor can be mainly interpreted as the coking source.

While importing the data during fog and clear period separately into the PMF model, similar factor profiles were found during the two periods as illustrated in Figs. S3 and S4. However, by applying the multiple linear regression (MLR) model to identify the contributions of each source, it showed the significant difference between different period. As illustrated in Fig. 3, during the haze period, vehicle emissions turned out to be the most important potential PAHs contributor (33.2%), followed by the coal and biomass combustion (32.5%), coking (25.5%) and petroleum spill and leakages (8.87%). Compared to the haze period, a significant reduction of contributions in vehicle emissions (from 33.2% to 13.8%) was found during the clear period while a slightly less contributions were found for the coal and biomass combustion (from 32.5% to 23.3%). It indicated that vehicle emissions made a dominant contribution to the accumulation of $PM_{2.5}$-bound PAHs. In addition, the variation of factor contribution between haze

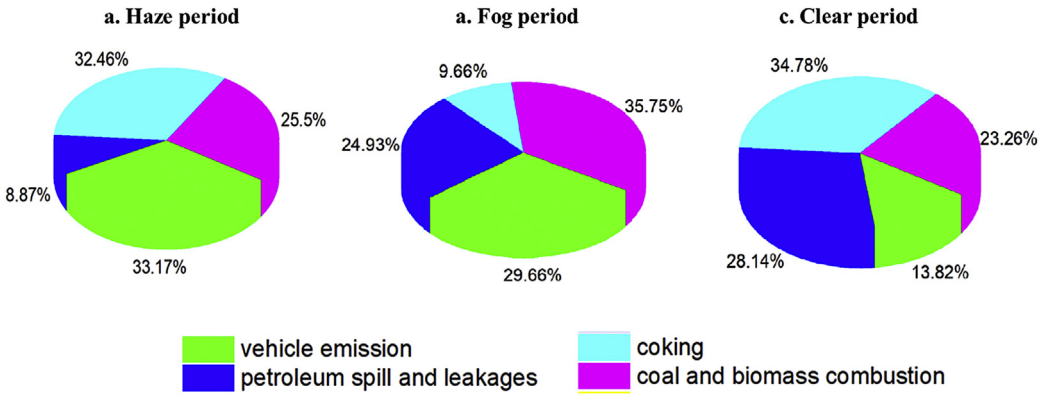

Fig. 3. Contributions of each factor to total PAH loadings in $PM_{2.5}$ during haze period (a), fog period (b), and clear period (c).

and fog period also indicated that the difference of each source was closely associated with weather conditions. For example, with the increase of relative humidity, the contribution of coal and biomass combustion decreased from 32.5% (haze) and 23.3% (clear) to 9.67% (fog), respectively, while the major source of PAH contaminations was petroleum spill and leakages during the fog period.

In comparison with three study periods, it can be confirmed that vehicle emission and coal, biomass combustion were the predominant sources to PAHs accumulation in the severe haze, which was in accordance with the results of other researches during similar study period on the $PM_{2.5}$ source identification in Shanghai (Wang et al., 2016; Liu et al., 2018). It mainly resulted from the industrial area in the north of sampling site (Wujing heat and power plant) as well as the coal used for domestic heating in winter through long-range transportation which led to the severe air pollution.

3.5. PSCF and CWT model

As long-range transportation of coal and biomass burning from the surrounding areas, it was far from enough to determine the source apportionment by only PMF model. Hence, the HYSPLIT model was used for tracking the long-range transportation of potential source areas and apportioning contributions in the following chapter.

Backward trajectories cluster during three different periods (haze, fog and clear) were illustrated Table S7. In terms of the clustering results during haze period, three clusters were determined and the northwest trajectory, coming from Jiangsu province, Western Shandong and Hebei provinces enjoyed the highest mean level of $PM_{2.5}$-bound PAHs (12.8 ng/m^3) and EC (9.41 μg/m^3) concentrations as well as the largest frequency (45.2%). The airflow originated from Shandong province was passing through Yellow sea before arriving in Shanghai. It accounted for the lowest ratio (25.2%) of the total trajectories, which also carried the lowest PAH concentrations (8.06 ng/m^3).

During the clear period, major trajectories can be classified into three categories, accounting for 22.6%, 63.1% and 14.3% of the total trajectories. Trajectory (1) WNW-air masses from west-northwest of the studying area, which had the lowest PAHs (7.84 ng/m^3) and EC (6.09 μg/m^3) concentrations and the moderate frequency; (2) NW- air masses from northwest of sampling site carried the highest level of PAHs and EC pollution (20.8 ng/m^3 and 7.51 μg/m^3, respectively) and the largest frequency; (3) NNW- air masses from north-northwest accounted for the lowest ratio of the total trajectories as well as the shorter transport pathway.

During the fog period, the airflow was mainly coming from the north-northwest (NNW) area which can be separately into the fast NNW and slow NNW clusters. The percentage of the fast one occupied 47.8% of the total trajectories while the slow one only accounted for 32.9%. The fast NNW cluster had the lowest PAHs (6.29 ng/m^3) and EC (2.02 μg/m^3) concentrations which can be attributed to the higher wind speed and longer transportation from the contaminant source. Air masses originated from Shanxi province, crossing over Henan, Anhui and Jiangsu province, which indicated the shortest transport pathway along with the relative lower PAHs (6.32 ng/m^3) and EC (2.27 μg/m^3) concentrations.

Total EC concentrations showed the decreasing trend as haze (8.04 μg/m^3) > clear (7.12 μg/m^3) > fog (2.54 μg/m^3), and PAH concentrations showed the trend as clear (17.5 ng/m^3) > haze (10.2 ng/m^3) > fog (6.35 ng/m^3). It indicated that the serious EC pollution occurred during the haze period may result from the long-range transportation of coal, biomass and petroleum combustion in northwest area of sampling site especially the Hebei, Shandong, Jiangsu province. In addition, the potential pollution source of PAHs may be more inclined to the local area as the surrounding coal-fired thermal power plant near the sampling site.

As illustrated in Fig. 4a and b, spatial distributions of potential source areas and transport pathways of PAHs and EC were calculated by PSAF model. The higher PSCF values for pollutants indicated the more remarkable potential source regions, which was represented by the color of legend. The deeper in red represented the higher level of pollution while the deeper in blue was on the opposite.

During the haze period, the high PSCF values for PAHs were distributed significantly at the surrounding regions of sampling site, including the north of Jiangsu, Anhui and Zhejiang provinces in the east. It implied that pollution level of PAHs was remarkably influenced by the transportation of contaminants from industrialized areas in the YRD. Moderate PSCF values were found in Jiangxi and Hunan provinces while weak values occurred in Shandong and Hebei provinces. It indicated that long range transportation also played an important role in the contributions of PAHs in Shanghai. In comparison with PAHs, the relatively lower PSCF values of EC were found in Zhejiang province and the north of Jiangsu province. Liaoning province and east of Inner Mongolia province were no longer the potential areas in terms of EC. In general, the spatial distribution was similar between PAHs and EC which indicated the similar potential source regions.

By comparing the haze period with fog period, the difference of potential source regions of PAHs can be seen as was illustrated in Fig. 4c. The high PSCF values were concentrated in the southeast of Jiangsu province and Yellow Sea areas. The high relative humidity may result in the dilution of pollutants concentration so the airflow originated from inland area had lower PSCF values in comparison with the haze period.

Except for the PSCF method, CWT values were also calculated to support the result of PSCF (Fig. 4d). In comparison with PSCF, CWT method had the advantage of distinguishing the moderate pollutant source from the strong one. For example, the high value in the east of Zhejiang and the north of Jiangsu indicated the main potential source region. Most air mass originated from the south of Shandong, passing over Jiangsu from north to south, and mixed with the local emission in Shanghai. In general, both PSCF and CWT algorithm indicated Zhejiang, Anhui and Jiangsu provinces as major potential source areas of contaminations.

4. Conclusion

In this study, the temporal variations and potential source of PAHs and carbonaceous aerosols during severe haze episode were revealed in Shanghai. Overall, the higher accumulation of carbonaceous aerosols mainly appeared in the typical haze episodes with heavy vehicle emissions and intensive industrial pollutions. The correlation analysis elucidated significant correlations between carbonaceous aerosols and HMW PAHs, particularly during the haze period. Meanwhile, temperature was the most crucial meteorological factor while haze events were also driven by relative humidity. The stagnant weather and lower wind speed provided a favourable condition for the accumulation of pollutants and formation of the haze episode. In addition, OC_{pri} and OC_{sec} contributions were closely related to the haze severity extent. SOC, as the main aerosols resulting in heavy haze in Shanghai, accounted for 52.22% OC_{TOC} during the severe haze episode. The PMF model identified vehicle emissions and coal, biomass combustion as the two predominant sources of PAHs in Shanghai. HYSPLIT model clustered the trajectories of PAHs and carbonaceous aerosols in $PM_{2.5}$ along with the PSCF and CWT algorithm, which indicated Zhejiang, Anhui and Jiangsu provinces as major potential source areas of contamination. The comprehensive application of PMF and HYSPLIT model could be conducive to evaluate the potential source areas of PAH pollutions as well as controlling the corresponding contaminations based on the emission sources in advance.

Declarations of interest

None.

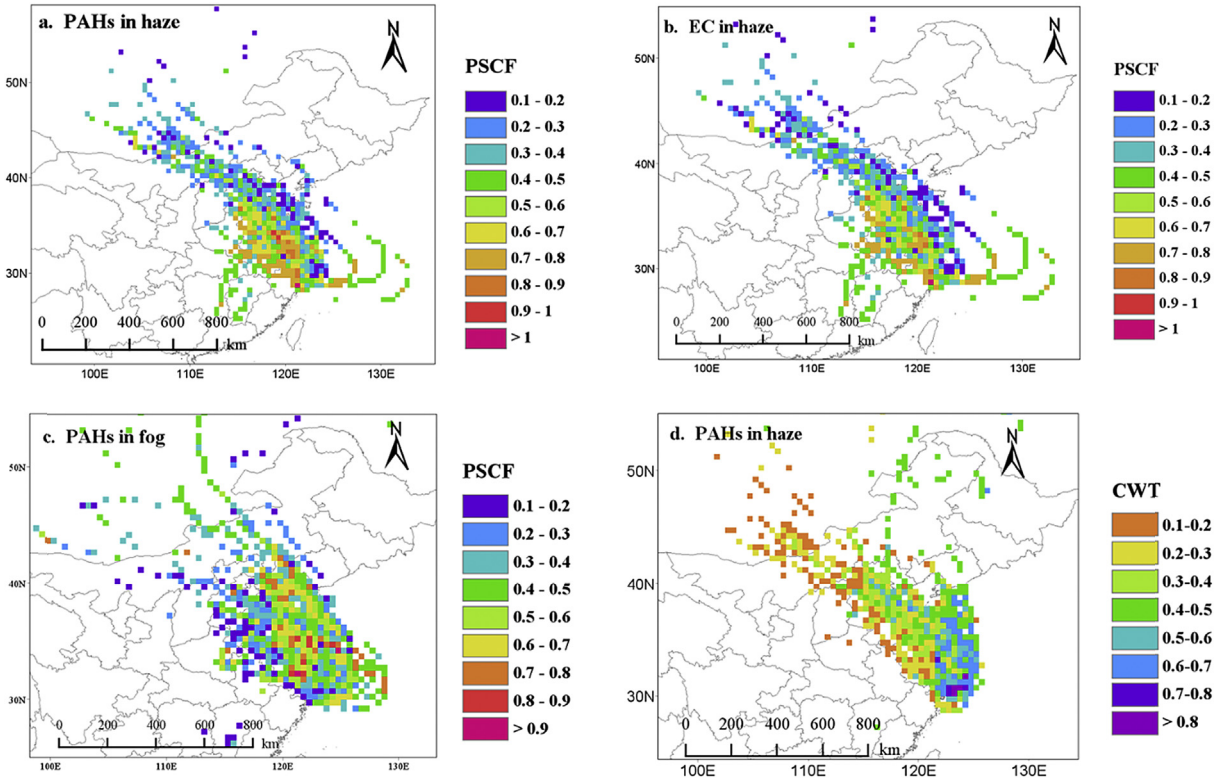

Fig. 4. PSCF values and spatial distribution of $PM_{2.5}$-bound PAHs during haze period (a). PSCF values and spatial distribution of $PM_{2.5}$-bound EC during haze period (b). PSCF values and spatial distribution of $PM_{2.5}$-bound PAHs during fog period (c). CWT values and spatial distribution of $PM_{2.5}$-bound PAHs during haze period (d).

Acknowledgments

The present study was financially supported by the National Natural Science Foundation of China (No. 41730646, 41761144062 and 41601526). Great thanks are given to our group members for their generous help in experiment and valuable advice on manuscript. We also acknowledge the editor and reviewers for their expert comments and suggestions.

Appendix A. Supplementary data

Supplementary data to this article can be found online at https://doi.org/10.1016/j.atmosenv.2019.01.046.

References

Aydin, Y.M., Kara, M., Dumanoglu, Y., Odabasi, M., Elbir, T., 2014. Source apportionment of polycyclic aromatic hydrocarbons (PAHs) and polychlorinated biphenyls (PCBs) in ambient air of an industrial region in Turkey. Atmos. Environ. 97, 271–285.

Barrado, A.I., García, S., Barrado, E., Perez, R.M., 2012. PM2.5-bound PAHs and hydroxy-PAHs in atmospheric aerosol samples: correlations with season and with physical and chemical factors. Atmos. Environ. 49, 224–232.

Blando, J.D., Turpin, B.J., 2000. Secondary organic aerosol formation in cloud and fog droplets: a literature evaluation of plausibility. Atmos. Environ. 34, 1623–1632.

Chen, D., Cui, H., Zhao, Y., Yin, L., Lu, Y., Wang, Q., 2017. A two-year study of carbonaceous aerosols in ambient PM2.5 at a regional background site for western Yangtze River Delta, China. Atmos. Res. 183, 351–361.

Chen, K., Yin, Y., Wei, Y.X., Yang, W.F., 2010. Characteristics of carbonaceous aerosols in PM2.5 in Nanjing. Zhongguo Huanjing Kexue/China Environmental Science 30, 1015–1020.

Chow, J.C., Watson, J.G., Chen, L.W.A., Arnott, W.P., Moosmüller, H., Fung, K., 2004. Equivalence of elemental carbon by thermal/optical reflectance and transmittance with different temperature protocols. Environ. Sci. Technol. 38, 4414–4422.

Chow, J.C., Watson, J.G., Louie, P.K.K., Chen, L.W.A., Sin, D., 2005. Comparison of PM2.5 carbon measurement methods in Hong Kong, China. Environ. Pollut. 137, 334–344.

Dimitriou, K., Kassomenos, P., 2015. Three year study of tropospheric ozone with back trajectories at a metropolitan and a medium scale urban area in Greece. Sci. Total Environ. 502, 493–501.

Gustafsson, Ö., Haghseta, F., Chan, C., MacFarlane, J., Gschwend, P.M., 1997. Quantification of the dilute sedimentary soot Phase: implications for PAH speciation and bioavailability. Environ. Sci. Technol. 31, 203–209.

Hildemann, L.M., Markowski, G.R., Cass, G.R., 1991. Chemical composition of emissions from urban sources of fine organic aerosol. Environ. Sci. Technol. 25, 744–759.

Huang, R., Zhang, Y., Bozzetti, C., Ho, K., Cao, J., Han, Y., Daellenbach, K.R., Slowik, J.G., Platt, S.M., Canonaco, F., Zotter, P., Wolf, R., Pieber, S.M., Bruns, E.A., Crippa, M., Ciarelli, G., Piazzalunga, A., Schwikowski, M., Abbaszade, G., Schnelle-Kreis, J., Zimmermann, R., An, Z., Szidat, S., Baltensperger, U., Haddad, I.E., Prévôt, A.S.H., 2014. High secondary aerosol contribution to particulate pollution during haze events in China. Nature 514, 218.

Joseph, A.E., Unnikrishnan, S., Kumar, R., 2012. Chemical characterization and mass closure of fine aerosol for different land use patterns in Mumbai city. Aerosol and Air Quality Research 12, 61–72.

Kong, S., Wen, B., Chen, K., Yin, Y., Li, L., Li, Q., Yuan, L., Li, X., Sun, X., 2014. Ion chemistry for atmospheric size-segregated aerosol and depositions at an offshore site of Yangtze River Delta region, China. Atmos. Res. 147–148, 205–226.

Kulkarni, P., Venkataraman, C., 2000. Atmospheric polycyclic aromatic hydrocarbons in Mumbai, India. Atmos. Environ. 34, 2785–2790.

Li, A., Jang, J., Scheff, P.A., 2003. Application of EPA CMB8.2 model for source apportionment of sediment PAHs in lake calumet, chicago. Environ. Sci. Technol. 37, 2958–2965.

Li, C.K., Kamens, R.M., 1993. The use of polycyclic aromatic hydrocarbons as source signatures in receptor modeling. Atmospheric Environment Part A. General Topics 27, 523–532.

Li, Y., Liu, X., Liu, M., Li, X., Meng, F., Wang, J., Yan, W., Lin, X., Zhu, J., Qin, Y., 2016. Investigation into atmospheric PM2.5-borne PAHs in Eastern cities of China: concentration, source diagnosis and health risk assessment. Environ. Sci.: Processes & Impacts 18, 529–537.

Liu, Y., Yu, Y., Liu, M., Lu, M., Ge, R., Li, S., Liu, X., Dong, W., Qadeer, A., 2018. Characterization and source identification of PM2.5-bound polycyclic aromatic hydrocarbons (PAHs) in different seasons from Shanghai, China. Sci. Total Environ. 644, 725–735.

Marr, L.C., Kirchstetter, T.W., Harley, R.A., Miguel, A.H., Hering, S.V., Hammond, S.K., 1999. Characterization of polycyclic aromatic hydrocarbons in motor vehicle fuels and exhaust emissions. Environ. Sci. Technol. 33, 3091–3099.

Motelay-Massei, A., Ollivon, D., Garban, B., Tiphagne-Larcher, K., Zimmerlin, I., Chevreuil, M., 2007. PAHs in the bulk atmospheric deposition of the Seine river basin: source identification and apportionment by ratios, multivariate statistical techniques and scanning electron microscopy. Chemosphere 67, 312–321.

Nicolás, J., Chiari, M., Crespo, J., Galindo, N., Lucarelli, F., Nava, S., Yubero, E., 2011. Assessment of potential source regions of PM2.5 components at a southwestern Mediterranean site. Tellus B: Chem. Phys. Meteorol. 63, 96–106.

Park, S.S., Cho, S.Y., Kim, K., Lee, K., Jung, K., 2012. Investigation of organic aerosol sources using fractionated water-soluble organic carbon measured at an urban site. Atmos. Environ. 55, 64–72.
Pio, C., Cerqueira, M., Harrison, R.M., Nunes, T., Mirante, F., Alves, C., Oliveira, C., Sanchez De La Campa, A., Artíñano, B., Matos, M., 2011. OC/EC ratio observations in Europe: Re-thinking the approach for apportionment between primary and secondary organic carbon. Atmos. Environ. 45, 6121–6132.
Schauer, C., Niessner, R., Poschl, U., 2003. Polycyclic aromatic hydrocarbons in urban air particulate matter: decadal and seasonal trends, chemical degradation, and sampling artifacts. Environ. Sci. Technol. 37, 2861–2868.
Simcik, M.F., Eisenreich, S.J., Lioy, P.J., 1999. Source apportionment and source/sink relationships of PAHs in the coastal atmosphere of Chicago and Lake Michigan. Atmos. Environ. 33, 5071–5079.
Smith, K.R., Jerrett, M., Anderson, H.R., Burnett, R.T., Stone, V., Derwent, R., Atkinson, R.W., Cohen, A., Shonkoff, S.B., Krewski, D., Pope, C.A., Thun, M.J., Thurston, G., 2009. Public health benefits of strategies to reduce greenhouse-gas emissions: health implications of short-lived greenhouse pollutants. Lancet 374, 2091–2103.
Sofowote, U.M., McCarry, B.E., Marvin, C.H., 2008. Source apportionment of PAH in Hamilton harbour suspended sediments: comparison of two factor Analysis methods. Environ. Sci. Technol. 42, 6007–6014.
Tan, J., Guo, S., Ma, Y., Duan, J., Cheng, Y., He, K., Yang, F., 2011. Characteristics of particulate PAHs during a typical haze episode in Guangzhou, China. Atmos. Res. 102, 91–98.
Tsang, T.T.H., Pai, P., Korgaonkar, N.V., 1988. Effect of temperature, atmospheric condition, and particle size on extinction in a plume of volatile aerosol dispersed in the atmospheric surface layer. Appl. Optic. 27, 593–598.
Turpin, B.J., Huntzicker, J.J., 1995. Identification of secondary organic aerosol episodes and quantitation of primary and secondary organic aerosol concentrations during SCAQS. Atmos. Environ. 29, 3527–3544.
Vander Wal, R.L., Yezerets, A., Currier, N.W., Kim, D.H., Wang, C.M., 2007. HRTEM Study of diesel soot collected from diesel particulate filters. Carbon 45, 70–77.
Wang, Q., Liu, M., Yu, Y., Du, F., Wang, X., 2014. Black carbon in soils from different land use areas of Shanghai, China: level, sources and relationship with polycyclic aromatic hydrocarbons. Appl. Geochem. 47, 36–43.
Wang, Q., Liu, M., Yu, Y., Li, Y., 2016. Characterization and source apportionment of PM2.5-bound polycyclic aromatic hydrocarbons from Shanghai city, China. Environ. Pollut. 218, 118–128.
Wang, Y.Q., Zhang, X.Y., Draxler, R.R., 2009. TrajStat: GIS-based software that uses various trajectory statistical analysis methods to identify potential sources from long-term air pollution measurement data. Environ. Model. Softw 24, 938–939.
Yang, F., Huang, L., Duan, F., Zhang, W., He, K., Ma, Y., Brook, J.R., Tan, J., Zhao, Q., Cheng, Y., 2011. Carbonaceous species in PM2.5 at a pair of rural/urban sites in Beijing, 2005–2008. Atmos. Chem. Phys. Discuss. 11, 7893–7903.
Zhang, Y.L., Huang, R.J., El Haddad, I., Ho, K.F., Cao, J.J., Han, Y., Zotter, P., Bozzetti, C., Daellenbach, K.R., Canonaco, F., Slowik, J.G., Salazar, G., Schwikowski, M., Schnelle-Kreis, J., Abbaszade, G., Zimmermann, R., Baltensperger, U., Pr Ev Ot, A.S.H., Szidat, S., 2015. Fossil vs. non-fossil sources of fine carbonaceous aerosols in four Chinese cities during the extreme winter haze episode of 2013. Atmos. Chem. Phys. 15, 1299–1312.
Zhou, M., Chen, C., Qiao, L., Lou, S., Wang, H., Huang, H., Wang, Q., Chen, M., Chen, Y., Li, L., Huang, C., Zou, L., Mu, Y., Zhang, G., 2013. The chemical characteristics of particulate matters in Shanghai during heavy air pollution episode in Central and Eastern China in January 2013. Huanjing Kexue Xuebao/Acta Sci. Circumstantiae 33, 3118–3126.